Effect of initial height on dynamics and instability of vortex-ring/wall interaction

Heng Ren

***Abstract*— The interaction of a vortex ring with a flat wall at $\mathrm{Re}=4\times10^4$ in three dimensions is investigated using large eddy simulation (LES). We consider the effect of initial height of a vortex ring. For low height case, the secondary vortex ring moves far away from the wall with strong strength. While for high height case, the strength of the secondary ring is weak and large deformation occurs for it. The dominant mode for both primary and secondary vortex rings is n=6 and we find the instability for high height case grows more rapidly than for the low height case. In the late stage of interaction, the strong vortex-vortex and vortex-wall interactions lead to the large vortex structures breakdown into small scale vortices and the flow transfers to turbulence. The fully turbulent flow is marked by the same order of magnitude of perturbation energy for low modes and the -5/3 decay law of perturbation kinetic energy spectra.**

***Index Terms*— Vortex ring, flat wall, large eddy simulation, instability.**

[1] INTRODUCTION

The interaction of vortical structures with solid boundaries is a fundamental fluid dynamic topic which has received considerable attention in recent years. The interest in this subject is partly due to several practical applications, (e.g. impact of helicopter rotor vortices with following rotor blades or with the vehicle airframe, chopping of a pump intake vortex by the turbine blades, and interaction of an aircraft trailing vortex with a following aircraft or with the airstrip during landing and take-off), and partially in order to gain a better insight in the fundamental dynamics of vorticity in such flow situations. As one of the simplest and important forms of vortex motion, vortex rings widely exist in nature. The interaction of vortex rings with solid boundaries is an important problem in fluid dynamics. This subject is also associated with a variety of practical applications, such as vortex rings extinguishing gas and oil well fires [1], cavitated rings used for underwater drilling [2], and modeling the interaction between the downburst and the aircraft [3]. Moreover, the underlying flow phenomena and physical mechanisms are still unclear and are of great interest for detailed studies.

Vortex rings interacting with a flat wall has been extensively studied. These studies [4-9] showed that as the primary vortex ring moves gradually toward the wall, its rate of approach slows and its radius continues to increase; meanwhile, considerable secondary vorticity is generated on the surface. When the Reynolds number, based on the initial diameter and translational speed of the vortex ring, is larger than about 500, the secondary vorticity separates from the surface and interacts with the primary vortex ring resulting in the ring rebounding from the wall. Actually, these studies are mainly limited to relatively low Reynolds numbers, the highest Reynolds number in these studies is about 2840 [9]. The experimental study [9] has revealed that, beyond *Re* = 3000 for the interaction between a vortex ring and a flat wall, the primary vortex ring will no longer remain stable as it approaches the wall.

For the instability of a free vortex ring, there are theoretical, experimental, and numerical studies [10-11]. While the azimuthal instability of a vortex ring impinging on a solid wall has been examined, to our knowledge, only in the experimental study by Walker et al. [9] and numerical studies by Olandi et al. [6]. In this letter, we investigate the effect of initial height of a vortex ring on the dynamics and instability of vortex-ring/wall interaction.

[2] NUMERICAL METHOD

To investigate a vortex ring impinging on a curved surface, the three-dimensional Favre-filtered compressible Navier-Stokes equations in generalized coordinates are employed. The equation of state for an ideal gas is used and the molecular viscosity is assumed to obey the Sutherland law. To non-dimensionalize the governing equations, the radius of the initial vortex ring and the far-field variables are used as characteristic quantities. It should be indicated that, similar to LES on the evolution of longitudinal stationary vortices [12], the present simulation is for a low Mach number of 0.3 based on the far-field speed of sound, which is very near the incompressible limit. Sreedhdar and Ragab [12] have verified that the approach based on the compressible N-S equations can reliably predict the incompressible flow characteristics of the vortex evolution.

The large eddy simulation is implemented for turbulence closure. In order to model some terms in the Favre-filtered equations arising from the unresolved scales, dynamic subgrid-scale (SGS) models for turbulent flows are employed. A detailed description of the mathematical formulation of the governing equations and the SGS models have been given in our previous paper [13-14].

The governing equations are numerically solved by a finite-volume method. As employed in our previous work [13-14], the convective terms are discretized by a second-order central scheme and the viscous terms by a fourth-order centered scheme. Time advancement is

Manuscript received January, 2016.

***Heng Ren**, China Electronics Technology Group Corporation No.38 Research Institute, Hefei, China, +86 18900518514.*

ISSN: 2278 – 7798

performed by an implicit approximate factorization method with sub iterations to ensure a second-order accuracy. Moreover, the present numerical methods have already been used successfully to a variety of turbulent flows and have been verified to provide the reliable calculations.

[3] COMPUTATION MODEL AND BOUNDARY CONDITIONS

As illustrated in Fig. 1, a vortex ring of radius R_0 is initially placed at $\boldsymbol{x_c}$ = (0, 0, h), h is the distance between the vortex ring center and the wall.

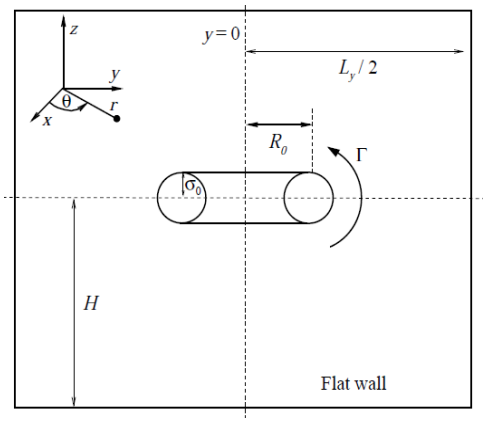

Fig. 1. Schematic diagram of a vortex ring approaching a flat wall.

The initial vorticity distribution of the vortex ring is assigned by a Gaussian function. The initial translational speed of the vortex ring can be represented as

$$u_v = \frac{\Gamma}{4\pi R_0}(\ln\frac{8R_0}{\sigma_0} - \frac{1}{4}), \qquad (1)$$

where σ_0 is the initial core radius and Γ is the circulation of the vortex ring. To deal with the instability of the vortex ring, an azimuthal disturbance with an amplitude of 2×10^{-4} is introduced by imposing a radial displacement on the axis of the ring.

In the computation, we calculate two cases with h = $9R_0$ and $12R_0$ respectively. For both cases, slenderness ratio of the vortex ring is $\sigma_0 / R_0 = 0.4$ and the initial translational speed of the ring is $u_s = 0.3$. Reynolds number based on the translational speed and ring diameter is $Re = 4 \times 10^4$, and the corresponding Reynolds number based on circulation of the vortex ring is $Re_\Gamma = 9.15 \times 10^4$. After the two cases have evolved for time t_0=23 and t_0=35 respectively, the vortex ring for both cases reaches z=$3R_0$, which is high enough and the effect of wall on the vortex ring is little. In order to compare the results of two cases at a special time, we use t-t_0 to define the time.

The computational domain extends for 16 ring radii in the x and y directions and 12 radii in the vertical direction, with $L_x/R_0 = L_y/R_0 = 16$, $L_z/R_0 = 12$. Based on our careful examinations, a mesh of size $N_x \times N_y \times N_z = 641 \times 641 \times 263$ with resolution $R_0 = 40\Delta x$ is used in the computation, where N_x and N_y are dimensions of the mesh in two horizontal directions x and y, and and N_z is the dimension in the vertical direction z. The grid-spacing is uniform in x and y, and grid stretching is employed in z to increase the grid resolutions near the surface. In the transversal x and y directions, periodicity boundary conditions are used. In the vertical z direction, the flow is bounded by a no-slip wall on the bump surface and far-field boundary condition at $z = L_z$.

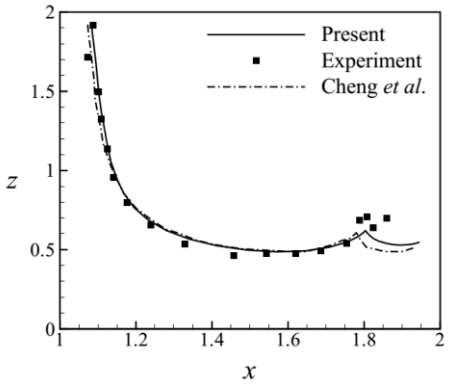

Fig. 2. The trajectory of the primary ring center for Re = 830. The solid and dashdot lines present the numerical results obtained in this work and by Cheng *et al*. respectively. The symbol represents the experimental data.

We will validate our code by a comparison with the existing results for a vortex ring impacting a flat wall at Re = 830. For the vortex ring/wall interacting case, the initial conditions are the same with experiment by Chu *et al*. [8]. The Gaussian ring is initially placed at the vertical position h = $3R_0$ and we use the grid resolution $R_0 = 30\Delta x$ for the simulation which is same with the cases in Cheng *et al*. [4]. We compare the trajectory of the primary vortex ring center with the experiment and the numerical study, as shown in Fig. 2. Clearly, our results are convergent to the experimental data and better than numerical results by Cheng *et al*. using Lattice Boltzmann method.

[4] RESULTS AND DISCUSSION

We first discuss the complex flow structures. Figure 3 shows the evolution of three-dimensional vortex structures depicted by isosurface of the Q-criterion for the two cases. A sequence of events takes place when a vortex ring approaches a flat wall. Firstly, when the vortex ring is close to the wall, the ring entrains surrounding fluids and a thin boundary layer is generated on the surface. Secondly, as the ring moves closer to the wall, it begins to stretch and the induced boundary layer grows rapidly. And thirdly, after t-$t_0 \geq 10$, the boundary layer undergoes separation in the adverse pressure gradient region leading to ejection of vorticity generated on the surface into the surrounding fluid. At t-t_0=15, we observe a second vortex ring is generated. It lifts up from the wall and then interacts with the primary ring. The interaction between the primary and secondary rings decelerates the radial expansion of the primary ring and causes the primary ring to rebound from the wall. At t-t_0=35, we observe the secondary vortex ring is moving far away from the wall and it develops into a wavy structure, which is mainly due to the growth of azimuthal instability. For h=$9R_0$ case, the wavy second vortex ring is visible and we observe a large number of vortices wrapping around the primary and secondary rings respectively. While for h=$12R_0$ case, the strength of the secondary ring is weak and large deformation occurs for it. This is the main difference between the two cases. After

ISSN: 2278 – 7798

t-t_0=45, the strong vortex-vortex and vortex-wall interactions lead to breakdown of vortex structures into small-scale vortices and complex three-dimensional topological structures appear.

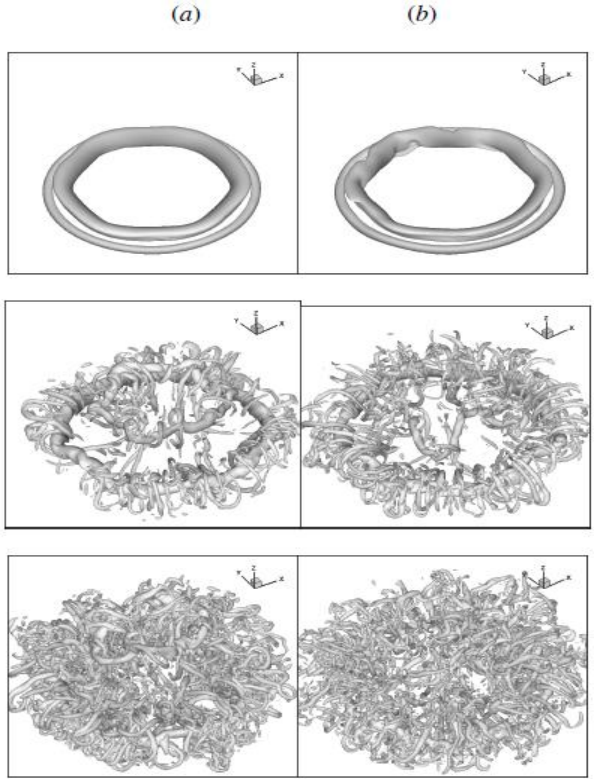

Fig. 3. Evolution of vortex structures shown by isosurface of the Q-criterion (Q=2). (a) h=9R_0, (b) h=12R_0. Evolution is from top to bottom and shown at times t-t_0 = 15; 35; 45.

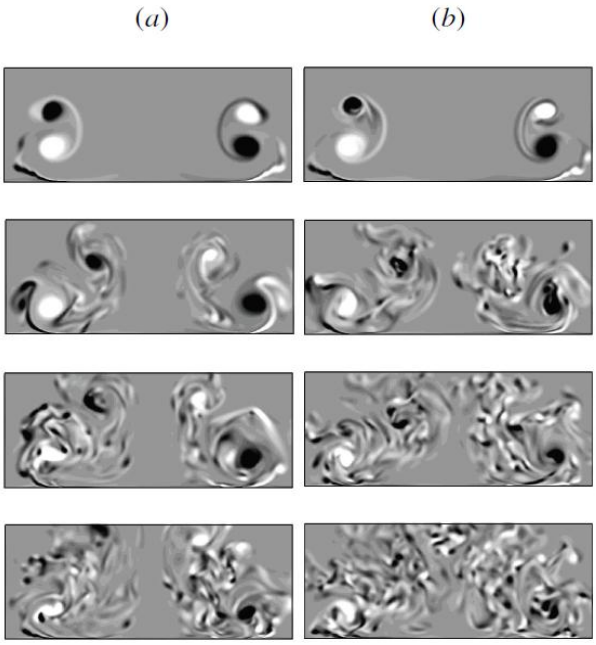

Fig. 4. The vorticity field in the y=0 plane. (a) h=9R_0, (b) h=12R_0. Evolution is from top to bottom and shown at times t-t_0 = 22; 35; 40; 45.

We give the vorticity field in the y=0 plane, as shown in figure 4. At t-t_0=22, the secondary vortex ring locates above the primary ring and the difference between the two cases is small. Then at t-t_0=35, we observe the breakdown of secondary vortex ring begins for h=12R_0. While for h=9R_0 case, the vorticity of secondary ring is quite strong. Finally, the secondary vortex ring for h=9R_0 has moved far away from the wall at t-t_0=45. At the same time, the secondary ring for h=12R_0 has broken into small-scale vortices. The difference between the two cases is more clearly shown by the averaged azimuthal vorticity in figure 5.

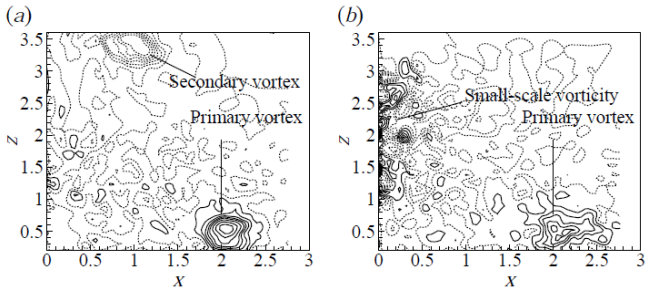

Fig. 5. The isocontours of azimuthally averaged vorticity at t - t_0=45. (a) h=9R_0, (b) h=12R_0.

We then discuss the evolution of kinetic energy and circulation of the primary vortex ring for two cases, as shown in figure 6. Before t - t_0 = 4, the vortex ring is far from the wall and the energy is almost constant. Then with the vortex ring moving closer to the wall, the energy decreases monotonically and slowly mainly due to the viscous dissipation of the flow. After the vortex ring collides with the wall at t - t_0=12, the kinetic energy begins to decrease rapidly. After t - t_0=22, we observe the energy for h=12R_0 decreases more rapidly than h = 9R_0. This implies the complicated vortex-vortex interaction for h = 12R_0 is stronger than h=9R_0 case. For the circulation of primary vortex ring, the strength for h = 12R_0 decays more rapidly after the ring interacts with the wall. This is mainly due to the stronger interaction between the primary ring and the wall and is consistent with the evolution of kinetic energy shown in figure 6 (a).

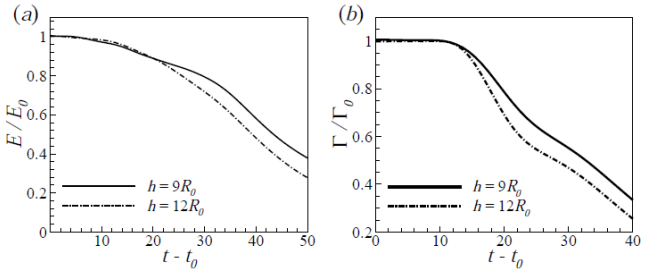

Fig. 6. Evolution of integrated kinetic energy (a) and circulation of primary vortex ring (b) for two cases.

Finally, we discuss the instability of vortex structures in the flow. The main instability mechanism of the vortex ring is an azimuthal instability. To ascertain the character of unstable waves, several mode shapes of the vertical vorticity for h = 9R_0 case at t - t_0 = 12 are plotted in figure 7. The dominant mode usually has the maxima azimuthal component of the vertical vorticity. It is apparent that n=6 is the dominant mode. This is consistent with the theoretical estimate of the most amplified azimuthal mode $n = 2.26/\sigma_0$ by Shariff et al. and the numerical results by Archer et al..

Azimuthal FFTs of the velocities, followed by an integration of the energy in the r-θ plane and averaged in the vertical direction, we obtain the perturbation kinetic energy spectra. The evolution of energy E_n for primary and secondary rings is present in figure 8. When the vortex ring

ISSN: 2278 – 7798

approaches the wall (t<37), only the energy of low modes increases. After the ring collides with the wall, at t=45, the energy increases considerably for all modes. At the same time, we observe the amplification of subharmonics (n=12,18,24) of the dominant mode n=6. Then the energy for all the modes decreases. At t=60, the low modes have reached the same order of magnitude. This marks the transition to turbulence. Finally, at t=70, the law of energy decay is a characteristic $n^{-5/3}$ law indicating that the turbulent mixing is saturate. For the secondary vortex ring, at t=37, corresponding to the time the generation of secondary ring begins, the large amplitude for low modes is due to adaptation of the instability. Then the behavior of perturbation kinetic energy is similar to the energy of primary vortex ring including the increase of all modes and the -5/3 decay law.

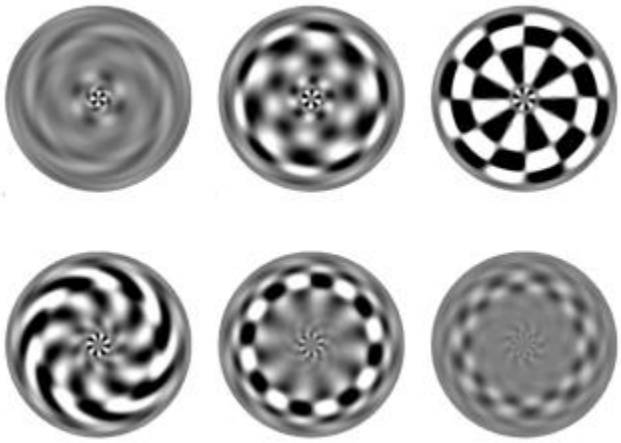

Fig. 7. Decomposition of modes of primary vortex ring for h = $9R_0$ case at t - t_0=12.

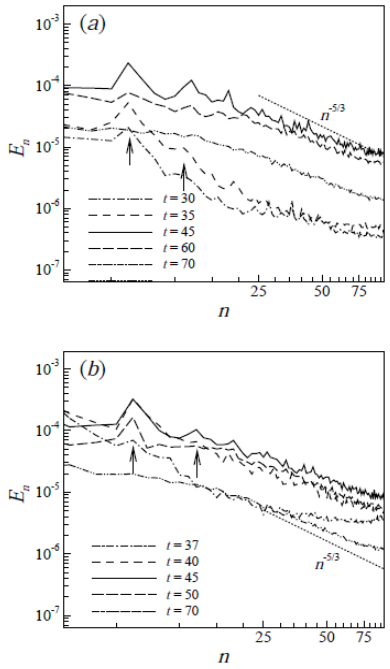

Fig. 8. Perturbation kinetic energy distribution over the all simulated modes at different times for h=$9R_0$ case. (a) Primary vortex ring, (b) secondary vortex ring. The energy peaks corresponding to the dominant and harmonic modes are identified with arrows.

The evolution of the most energetic azimuthal mode (n=6) for two cases is shown in figure 9. The energy of primary vortex ring for h=$12R_0$ grows more rapidly than h=$9R_0$ before the ring collides with the wall. At t-t_0=12, corresponding to the time the secondary vortex ring is separating from the wall. The induced velocity field by the secondary vortex ring leads to the higher growth rate of the primary ring. At t-t_0=18, for both cases, the peak value of perturbation energy for secondary ring is higher than primary ring. This implies the secondary vortex ring is more unstable and easier to break down than the primary ring. For the two cases, the higher amplitude of energy for secondary vortex ring in h=$12R_0$ case explains the large deformation of secondary ring in figure 3 (t-t_0=35). Then the energy of primary and secondary rings begins to decay and converges to a same value 10^{-5} at t-t_0=50, indicating the flow has transferred to turbulence.

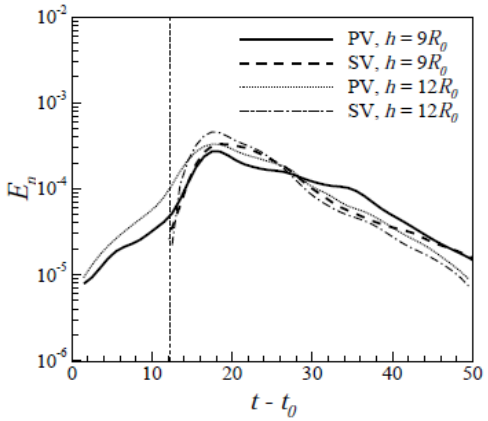

Fig. 9. Evolution of the most energetic azimuthal mode (n=6) for the two cases. PV and SV represent the primary and secondary vortex rings respectively.

[5] CONCLUSION

The interaction between a vortex ring and a flat plate has been studied by means of the large eddy simulation technique. The vortical flow phenomena and the underlying physical mechanisms were investigated and are summarized briefly as follows.

We investigate the effect of initial height of a vortex ring on the dynamics and instability of vortex structures. For h=$9R_0$ case, the secondary ring moves far away from the wall with strong strength. While for h = $12R_0$ case, large deformation and breakdown of secondary vortex ring occurs. This is mainly due to the higher growth rate of perturbation in secondary ring for h=$12R_0$ case. The dominant mode for both primary and secondary rings is n = 6 and is consistent with the previous results. The fully turbulent flow is marked by the same order of magnitude of perturbation energy for low modes and the -5/3 decay law of perturbation kinetic energy spectra.

REFERENCES

[1] D. G. Akhmetov, B. A. Lugovtsov, and V. F. Tarasov, "Extinguishing gas and oil well fires by means of vortex rings," *Combust. Explos. Shock Waves*, vol. 16, pp. 490-494, 1980.

[2] G. L. Chahine, and P. F. Genoux, "Collapse of a cavitating vortex ring," *J. Fluid Eng.*, vol. 105, pp. 400-405, 1983.

[3] T. S. Lundgren, and N. N. Mansour, "Vortex ring bubbles," *J. Fluid Mech.*, vol. 224, pp. 177-196, 1991.

ISSN: 2278 – 7798

[4] M. Cheng, J. Lou, and L. S. Luo, "Numerical study of a vortex ring impacting a flat wall," *J. Fluid Mech.*, vol. 660, pp. 430-455, 2010.
[5] T. T. Lim, T. B. Nickels, and M. S. Chong, "A note on the cause of rebound in the head-on collision of a vortex ring with a wall," *Exp. Fluids.*, vol. 12, pp. 41-48, 1991.
[6] P. Orlandi, and R. Verzicco, "Vortex rings impinging on walls: axisymmetric and three dimensional simulations," *J. Fluid Mech*., vol. 256, pp. 615-646, 1993.
[7] A. M. Naguib, and M. M. Koochesfahani, "On wall-pressure sources associated with the unsteady separation in a vortex-ring/wall interaction," *Phys. Fluids.*, vol. 16, pp. 2613-2622, 2004.
[8] C. C. Chu, C. T.Wang, and C. C. Chang, "A vortex ring impinging on a solid plane surface-Vortex structure and surface force," *Phys. Fluids A*, vol. 7, pp. 1391-1401, 1995.
[9] J. D. A. Walker, C. R. Smith, A. W. Cerra, and T. L. Doligalski, "The impact of a vortex ring on a wall," *J. Fluid Mech.*, vol. 181, pp. 99-140, 1987.
[10] P. G. Saffman, "The number of waves on unstable vortex rings," *J. Fluid Mech*., vol. 84, pp. 625-639, 1978.
[11] K. Shariff, R. Verzicco, and P. Orlandi, "A numerical study of three-dimensional vortex ring instabilities: viscous corrections and early nonlinear stage," *J. Fluid Mech*., vol. 279, pp. 351-375, 1994.
[12] M. Sreedhdar, and S. Ragab, "Large eddy simulation of longitudinal stationary vortices," *Phys. Fluids*, vol. 6, pp. 2501-2514, 1994.
[13] H. Ren, and X.Y. Lu, "Large eddy simulation of a vortex ring impinging on a three-dimensional circular cylinder," *Theor. Appl. Mech. Lett.*, vol. 3, 032007, 2013.
[14] H. Ren, and C. Y. Xu, "Three-dimensional numerical simulation of a vortex ring impacting a bump," *Theor. Appl. Mech. Lett.*, vol. 4, 032004, 2014.

Heng Ren received B. E. degree in Engineering Mechanics from Lanzhou University and Ph. D degree in Engineering Mechanics from University of Science and Technology of China. Presently working as an engineer in China Electronics Technology Group Corporation No.38 Research Institute. His research areas are electronic equipment thermal control and computational fluid dynamics.

ISSN: 2278 – 7798